DOE/ET-53088-352 IFSR #352

Numerical Investigation of a Plasma Beam Entering Transverse Magnetic Fields

J. Koga, J. L. Geary, T. Tajima

Institute for Fusion Studies
The University of Texas at Austin
Austin, Texas 78712

and

N. Rostoker

Department of Physics
University of California, Irvine
Irvine, California 92717

November 1988

NUMERICAL INVESTIGATION OF A PLASMA BEAM ENTERING TRANSVERSE MAGNETIC FIELDS

J. Koga* J.L. Geary T. Tajima

Institute for Fusion Studies

The University of Texas at Austin

Austin, Texas 78712

and

N. Rostoker

Department of Physics

University of California, Irvine

Irvine, California 92717

*Present address: Department of Space Science, Southwest Research Institute, 6220 Culebra Rd., San Antonio, Tx 78284

ABSTRACT

We study plasma beam injection into transverse magnetic fields using both electrostatic and electromagnetic particle-in-cell (PIC) codes. In the case of small beam momentum or energy (low drift kinetic β) we study both large and small ion gyroradius beams. Large ion gyroradius beams with a large dielectric constant $\epsilon \gg (\frac{M}{m})^{\frac{1}{2}}$ are found to propagate across the magnetitc field via $E \times B$ drifts at nearly the initial injection velocity, where $\epsilon = 1 + \frac{\omega_{pi}{}^2}{\Omega_i{}^2}$ and $\frac{M}{m}$ is the ion to electron mass ratio. Beam degradation and undulations are observed in agreement with previous experimental and analytical results. When ϵ is on the order of $(\frac{M}{m})^{\frac{1}{2}}$, the plasma beam propagates across field lines at only half its initial velocity and loses its coherent structure. When ϵ is much less than $(\frac{M}{m})^{\frac{1}{2}}$, the beam particles decouple at the magnetic field boundary, scattering the electrons and slightly deflecting the ions. For small ion gyroradius beam injection a flute type instability is observed at the beam magnetic field interface. In the case of large beam momentum or energy (high drift kinetic β) we observe good penetration of a plasma beam which shields the magnetic field from the interior of the beam (diagmagnetism).

1 INTRODUCTION

The general problem of plasma injection into magnetic fields has been an early and fundamental problem in plasma physics. Many experimental and theoretical studies have been devoted to the investigation of plasma stream interaction with curved and transverse magnetic fields. The reason for this interest is the many applications which this problem has. In fusion it has applications to the injection of plasma beams into magnetic confinement devices such as a tokamak or magnetic bottle. In laser experiments there are applications to the study of the dynamics of debris from laser targets streaming transverse to large magnetic fields (see Ripin et. al. 1987). Interest also exists in the area of space physics in the study of the interaction of the solar wind with artificial cloud releases for example AMPTE and the interaction of artificial beams with the geomagnetic field for example PORCUPINE (Haerendel and Sagdeev 1981).

The first study of plasma motion across magnetic fields was done by Chapman and Ferraro 1931 who studied the interaction of the solar wind and geomagnetic field. In an experiment Baker and Hammel 1962 demonstrated that a plasma beam could traverse a transverse magnetic field region via $\vec{E} \times \vec{B}$ drifts. The first theoretical study of plasma motion in curved magnetic fields was done by Schmidt 1960 who used the concept of space charge polarization to obtain equations for plasma motion. Schmidt found that a plasma beam with sufficient kinetic energy density, $\epsilon \gg 1$, where $\epsilon = 1 + \frac{{\omega_{pi}}^2}{{\Omega_i}^2}$ is the dielectric constant of the beam, ω_{pi} is the ion plasma frequency, and Ω_i is the ion gyrofrequency, would set up space charge layers in the beam as a result of ∇B drifts of the ions and electrons. These space charge layers set up a transverse electric field across the beam which allowed the beam to traverse the field via $\vec{E} \times \vec{B}$ drifts. Peter and Rostoker 1982 obtained expressions for the propagation velocity of large ion gyroradius beams across magnetic fields and found that beam propagation required $\epsilon \gg (\frac{M}{m})^{\frac{1}{2}}$ where $\frac{M}{m}$ is the ion to electron mass ratio. Small ion gyroradius beams have also been found capable of traversing magnetic fields by the Rayleigh-Taylor instability (see Peter 1981, Peter et. al. 1979).

Recent simulation studies have addressed many aspects of charge neutral beam dynamics in magnetic fields. Electrostatic simulations have been used to study instabilities which occur for small gyroradius beams streaming across magnetic fields (see Galvez 1987, Galvez et. al 1988). Humanic et. al. 1982 have simulated plasma cloud expulsion from large magnetic field regions for $\epsilon \gg 1$. Winglee and Prichett 1987 have simulated plasma injection at oblique angles to the magnetic field and have studied the effects of the electrons and ions streaming along field lines. Recent work in relation to the AMPTE Barium cloud release has addressed the problem of plasma cloud expansion into a uniform magnetic field with emphasis on the dynamics of flute formation along the cloud edges (Galvez et. al. 1988, Winske 1988). Papadopoulos et. al. 1988 have used hybrid simulations to study high drift kinetic β beam injection into magnetic fields where $\beta = \frac{4\pi n_b M u_0^2}{B^2}$, n_b is the beam density, M is the ion mass, u_0 is the beam drift velocity, and B is the magnetic field.

It is the purpose of this paper to study through particle simulation (see Hockney and Eastwood 1981, Birdsall and Langdon 1985, Tajima 1989) the effects of ϵ, ρ_i, and drift kinetic β on cross field propagation of charge neutral beams, where ρ_i is the ion gyroradius, $\rho_i = \frac{u_0}{\Omega_i}$.

2 TRANSVERSE INJECTION THEORY

Many theoretical papers have addressed the problem of plasma propagation across magnetic fields (see Schmidt 1960, Peter and Rostoker 1982, Treumann and Hausler 1985). So only a brief review of the basic propagation mechanisms will be given here. There are three ways in which a plasma beam drifting at a velocity u_0 can propagate across magnetic fields. First, for a large ion gyroradius beam, $a < \rho_i/4$, where a is the beam radius, a plasma beam can $\vec{E} \times \vec{B}$ drift across the field (Peter 1981, Peter et. al. 1979). Second, for $a \gg \rho_i$, small ion gyroradius beams, a plasma can propagate across field lines through the Rayleigh-Taylor instability. Third, for $\beta \gg 1$ the plasma beam has enough kinetic energy to push the magnetic field lines aside (ballistic motion).

This last mechanism is simple diamagnetism, which needs no further discussion. The former two mechanisms are briefly commented.

2.1 Large Ion Gyroradius Theory

When a plasma beam is injected across a magnetic field, the electrons and ions in the front portion of the beam initially move in opposite directions due to deflection by the Lorentz force. Space charge layers then build up on opposite sides of the beam forming an electric field which is transverse to the beam motion and the magnetic field lines(figure 1). This electric field $\vec{E}$ is approximately $\frac{\vec{u_0}\times\vec{B}}{c}$ (Schmidt 1960) where c is the velocity of light. The beam can then propagate through the magnetic field via $\vec{E}\times\vec{B}$ drifts if : $\epsilon \gg (\frac{M}{m})^{\frac{1}{2}}$, $a \gg \rho_i/\epsilon$(Peter 1981, Peter and Rostoker 1982), and $a < \rho_i/4$(Peter and Rostoker 1982, Lindberg 1978).

The first condition means that the drift kinetic energy density of the plasma must be greater than the electric field energy density created by the plasma and that charge neutrality be satisfied (Peter and Rostoker 1982).

The second condition requires the beam radius a to be greater than the space charge layer thickness ρ_i/ϵ. If space charge layers become significant in width with respect to the beam radius, then finite regions of charge buildup occur in the beam. The third condition is obtained from the assumption that the maximum potential difference that can be set up across the beam must be less than the initial ion kinetic energy (Peter and Rostoker 1982). It has been proposed (Lindberg 1978) that if the beam radius is larger than this value, the beam will split up into smaller beams in order to satisfy this condition.

When these conditions are met by the injected beam, the beam should propagate across the field. An analytic solution for the drift velocity of the beam was obtained for a collisionless plasma by Peter and Rostoker 1982: $u_x = u_0(1 - \frac{1}{\epsilon}(1 - cos(\sqrt{\epsilon}\Omega_h(t + \frac{x_0}{u_0})))) + O(\frac{1}{\epsilon^2})$ where $\Omega_h = (\Omega_e\Omega_i)^{\frac{1}{2}}$ is the hybrid gyrofrequency and x_0 identifies a particular fluid element initial position. In the limit of steady state and $\epsilon \gg 1$ this equation gives the result of Sinelnikov and

Rutkevich 1967. The wavelenth of this oscillation is on the order of $2\pi a_h/\sqrt{\epsilon}$ where a_h is the hybrid gyroradius, $\frac{u_0}{\Omega_h}$.

A time averaged value of the drift velocity is given by

$$u_x = u_0(1 - \frac{1}{\epsilon}). \tag{1}$$

For $\epsilon \gg 1$ the average drift velocity of the plasma through the field is nearly equal to the initial drift velocity of the plasma.

2.2 Small Ion Gyroradius Theory

For small ion gyroradius beams, $a \gg \rho_i$, it has been found (Wessel and Robertson 1981) that different depths of beam penetration occur depending on the quantity, $\frac{u_0}{\omega_{pi}}$, where ω_{pi} is the ion plasma frequency. This quantity is a measure of the distance over which charge separation can occur within the plasma.

A tenuous plasma beam satisfies the condition, $\frac{u_0}{\omega_{pi}} \gg \rho_i$ (Wessel and Robertson 1981). In this case the electrons and ions behave as individual particles. The depth of penetration is approximately equal to their respective gyroradii. The ions, therefore, penetrate further into the magnetic field than the electrons. Collective effects do not substantially alter single particle motion.

A dense beam satisfies the condition, $\frac{u_0}{\omega_{pi}} < a_h$ (Wessel and Robertson 1981). The equations of motion for the electrons and ions are closely coupled. Therefore, the depth of penetration for both species is a_h.

An intermediate beam satisfies the condition, $a_h < \frac{u_0}{\omega_{pi}} < \rho_i$ (Wessel and Robertson 1981). In this case the electron and ion motions are decoupled. The electrons turn around in a distance ρ_e where ρ_e is the eletron gyroradius, $\rho_e = \frac{u_0}{\Omega_e}$. The ions turn around at $\frac{u_0}{\omega_{pi}}$ due to a space charge set up.

Deeper penetration of a large ion gyroradius beam into magnetic fields is possible if the

beam breaks up into beamlets with width less than $\frac{\rho_i}{4}$ (Lindberg 1978). Then the beamlets can propagate across the magnetic field by $\vec{E} \times \vec{B}$ drifts. It has been shown (Peter 1981, Peter et. al. 1979) that the boundary between the front of the plasma and the magnetic field is unstable to the Rayleigh-Taylor instability. This instability may force break up the beam through the formation of flutes.

Also it should be noted that the dynamics of small ion gyroradius beams is similar to large ion gyroradius beams with shorted out polarization fields. Examples would include beam injection into a background plasma or beams hitting a metal container wall.

3 NUMERICAL METHODS

Both electrostatic and electromagnetic particle-in-cell (PIC) codes with explicit leapfrog time stepping (the so called Boris algorithm) are employed in the simulations. Both codes are $2\frac{1}{2}$ dimensional where two spatial coordinates (x,y) and three velocity coordinates (v_x, v_y, v_z) are calculated for each particle.

The simulation configuration is shown in figure 2. The size of the simulation region is normally $128\Delta \times 64\Delta$ in the x and y directions, respectively, where Δ is the grid size which is taken to be one.

A finite size beam is allowed to drift in the +x direction with different velocities and shapes. For all runs the particles had a size Δ of Gaussian charge distributions in both the x and y directions. Due to code conventions the electrons are positively charged and the ions are negatively charged. The particle thermal velocities are Maxwellian distributions in all directions.

An external magnetic field is applied in the z direction which is pointing out of the plane of the simulation box. The magnetic field B_z starts off at 0 at the left boundary until generally x=63Δ where it is increased parabolically to a maximum value within a few grid cells. After reaching its maximum value, the B_z field is held constant. Although this field is not curl free, its

existence can be attributed to a vacuum current which exists in the simulation box but doesn't interact with the plasma (see Humanic et. al. 1982).

In all the codes the boundary conditions are set up such that all field and particle quantities are periodic in the y direction. At the x boundaries conducting wall conditions are imposed on the fields and reflecting wall conditions are imposed on the particles. Test simulations with no magnetic field and half the simulation size in the y direction show that the conducting wall or periodic boundary conditions have little or no effect on beam propagation.

4 TRANSVERSE SIMULATION RUNS

Cross field simulations are carried out for beams with both $\beta < 1$ and $\beta \gg 1$ to determine beam injection characteristics with and without significant diamagnetic shielding. Low and high beta injection are studied using the electrostatic and electromagnetic codes respectively. The relevant parameters for each run are given in table 1.

4.1 Low β Injection

Low drift kinetic β beams with large and small ion gyroradii relative to the beam width are studied. Three types of large ion gyroradius beams are examined: $\epsilon \gg (\frac{M}{m})^{\frac{1}{2}}$, $\epsilon \approx (\frac{M}{m})^{\frac{1}{2}}$, and $\epsilon \ll (\frac{M}{m})^{\frac{1}{2}}$. For these simulations the simulation box is $128\Delta \times 64\Delta$ and the beam size is $50\Delta \times 5\Delta$ in the x and y directions respectively. In all of the simulation runs the beam is initially sent drifting in the +x direction. The magnetic field, B_z, is started from 0 at x=63Δ, allowed to increase parabolically until x=68Δ, and held constant from that point.

Figures 3 and 4 show particle and electric potential plots for $\epsilon \gg (\frac{M}{m})^{\frac{1}{2}}$(case 1 in Table 1). When the beam encounters the magnetic field, the ions and electrons at the front of the beam deflect in opposite directions due to the Lorentz force (figure 3a). This results in the polarization electric field which is set up across the front of the beam (figure 4a). Figure 4b shows that after

the beam has completely entered the field, the polarization field is set up along the length of the beam allowing the beam to $E \times B$ drift across the field. One noteworthy feature in the potential plots is the appearance of undulations along the beam. Since undulations in the potential reflect variations in the polarization electric field and the electric field is proportional to the drift velocity (Schmidt 1960), these undulations may reflect variation in the beam drift velocity. The wavelength of the undulations is between $9-12\Delta$, which is close to the predicted spatial variation 7.7Δ of the beam velocity from $2\pi a_h/\sqrt{\epsilon}$ (Peter and Rostoker 1982). The parabolic increase of the magnetic field over a distance of 5Δ may be responsible for the longer wavelength observed in the simulations. The variation length calculated by Peter and Rostoker 1982 was obtained with the assumption of a step function magnetic field. If the distance over which the magnetic field B_z rises were much longer than $\frac{u_0}{\omega_{pe}}$ which is 1.22Δ then these undulations may not have been observed (Ishizuka and Robertson 1982). The average drift velocity u_x of the beam through the magnetic field is about $6.93\omega_{pe}\Delta$. This is slightly lower than the velocity, $6.98\omega_{pe}\Delta$, as predicted from (1) where the initial drift velocity u_0 is $7\omega_{pe}\Delta$. Slight expansion of the beam before hitting the magnetic field may cause the actual dielectric constant ϵ of the beam to be smaller which results in a lower average drift velocity. The loss of electrons and ions from the edges of the beam is evident in figure 3. This beam degradation where the particles are lost from the charge layers at the edges of the beam has been observed in several experiments (Bostick 1956, Ishizuka and Robertson 1982).

Figures 5 and 6 show particle and potential plots for $\epsilon \approx (\frac{M}{m})^{\frac{1}{2}}$(case 2 in Table 1). As is evident from the both the electron and ion particle plots distortion of the beam occurs as soon as the magnetic field B_z is encountered (figures 5a,b). In the electron particle plots one can see the development of a vortex structure with radius $r \approx \rho_i$ (figures 5a,c,e). In figure 5b the ion particle plots show the development of a jet-like structure. This jet of ions can be attributed to a longitudinal electric field which has been set up along the front of the beam. The longitudinal field causes the ions at the front of the beam to reflect backwards. Reflected ions were detected

by Wessel and Robertson 1981 in an experiment where parameters were close to this simulation run. Beam degradation is much more extensive for this case than for $\epsilon \gg (\frac{M}{m})^{\frac{1}{2}}$. Also there are large regions of the beam which are not charge neutral. A large portion of the electrons and ions is left behind the front of the beam just before the magnetic field reaches its maximum. This result is expected since a large fraction of the beam should have too little energy to traverse the field region. As the beam electrons and ions penetrate deeper into the magnetic field the rectangular shape of the beam is lost (figure 5g,h). The potential is exhibiting both behavior for $\epsilon \gg (\frac{M}{m})^{\frac{1}{2}}$ where the transverse field is dominant and $\epsilon \ll (\frac{M}{m})^{\frac{1}{2}}$ where the longitudinal field at the front of the beam is dominant. The potential at time $\omega_{pe}t = 8.75$ indicates a mixture of longitudinal and transverse components for the electric field (fig. 6b). An asymmetric potential similar to that observed by Wessel and Robertson 1981 is shown in figure 6a in the initial injection phase of the simulation run. The peak potential is shifted toward the ions and can be attributed to the backstreaming ions (figure 5b). However, the potential later shifts towards the electrons (figure 6c). This may be attributed to the disruption of the beam and the tighter clumping of the electrons on one side of the beam. Figure 6c shows a transverse potential drop across the beam which indicates that a portion of the beam is $E \times B$ drifting across the magnetic field B_z. However, the penalty of this traversal is twofold. First, there is substantial particle loss degrading the beam shape. Second, the beam drift velocity is approximately half the initial drift velocity u_0. This low drift velocity is due to the fact that a large portion of the beam kinetic energy has been used creating the polarization field.

A simulation for $\epsilon \ll (\frac{M}{m})^{1/2}$ (case 3 in Table 1) shows that beam electrons are stopped immediately at the magnetic field boundary. The distance which they penetrate is approximately ρ_e. The electrons are scattered backward from the magnetic field region. On the other hand beam ions show little distortion from the original beam shape. The deflection of the ions indicates a turn around distance on the order of $\frac{u_0}{\omega_{pi}}$ or ρ_i which are equal in this simulation. This behavior

is similar to a small ion gyroradius beam of intermediate density where $a_h < \frac{u_0}{\omega_{pi}} < \rho_i$ (Wessel and Robertson 1981). The parameter $\frac{u_0}{\omega_{pi}}$ can be expressed in terms of ϵ as $\frac{u_0}{\omega_{pi}} = \frac{\rho_i}{\sqrt{\epsilon-1}}$. Using the value of ϵ in this simulation run $\frac{u_0}{\omega_{pi}}$ is approximately ρ_i. So the beam electrons and ions are decoupled and turn around within the distances seen in the simulation. A smaller value for ϵ would probably cause the ions to turn around within a distance of ρ_i satisfying the condition of a tenuous beam where $\frac{u_0}{\omega_{pi}} \gg \rho_i$ (Wessel and Robertson 1981).

For small ion gyroradius beam injection, the system size and magnetic field variation are the same as in the previous simulation runs. The beam size is changed to $30\Delta \times 30\Delta$ in the x and y directions. In this case $\frac{u_0}{\omega_{pi}}$ is less than a_h which satisfies the condition of a dense beam. The dielectric constant of the beam satisfies the condition: $\epsilon \gg (\frac{M}{m})^{\frac{1}{2}}$(case 4 in Table 1). Because of constraints on system size, the ion gyroradius ρ_i is only three times smaller than the beam width and length. Ideally ρ_i should be at least an order of magnitude smaller than any of the beam dimensions. However, simulation results show some aspects of wide beam behavior predicted by Peter et al. 1979. Particle plots in figure 7a and 7b show that the ions and electrons bunch up at the magnetic field boundary. Fig. 8b shows a periodic variation in E_y along the plasma beam magnetic field boundary with a wavelength, $\lambda \approx \rho_i$. This is indicative of the Rayleigh Taylor instability predicted by Peter et al. 1979. At a later time ion and electron particle plots in figures 7c and 7d show the formation of beamlets or flutes separated by distances roughly corresponding to ρ_i. After the instability has saturated at $\omega_{pe}t \approx 37$, particle plots at $\omega_{pe}t = 40$ and 50 show that the beamlets lose their individual shape and merge. Also at the same time the periodic structure in the E_y plots disappears. By the end of the simulation the beam has penetrated approximately $5a_h$ into the magnetic field. This is farther than the single a_h that a dense beam without the instability would have propagated. A simulation growth rate of $\gamma = 0.1\omega_{pe}$ is measured from the increase in the total electrostatic field energy until saturation. A growth rate $\gamma = 0.4\omega_{pe}$ is calculated from the formula by Peter et al. 1979. This discrepancy is not suprising considering the fact that the beam is not infinite as assumed in the Peter article, that the growth rate is

measured from summing over all modes of the instability, and that there is a finite ramp length over which the magnetic field B_z increases in the simulation.

4.2 High β Injection

Simulation runs are carried out to examine the effects of high drift kinetic β on high dielectric constant plasma beam injection across magnetic fields. Since for $\beta \gg 1$ bending and shielding of the magnetic fields are expected to become significant, electromagnetic codes are used. As in case 1 the beam is $50\Delta \times 5\Delta$ in the x and y directions respectively. The system size is increased to a $256\Delta \times 64\Delta$ grid in the x and y directions, respectively, to allow the beam more time in the transverse field region and to observe possible longtime plasma motions. The magnetic field B_z is turned on at x=64Δ, allowed to increase parabolically to a maximum value at x=69Δ, and kept constant from that point. Large ion gyroradius beams with $\beta = 130$ and $\beta = 65$ are studied.

As the beam enters the magnetic field with $\beta = 130$ (case 5 in Table 1) a transverse potential is observed to set up similar to the previous low β injection case. In figure 9 one can see particle plots for the electrons and ions when the entire beam is embedded in the magnetic field. The current plot in figure 10 shows the average J_x current profile across the beam. The actual current direction is opposite to the figure because of the reversed sign of the electrons and ions in the simulation code. A diamagnetic shielding current has set up on the edges of the beam counteracting the magnetic field. Figure 11 shows the plasma beam contribution to the transverse B_z field. The magnetic field is partially shielded out from a large part of the interior of the plasma beam. At the back of the beam a maximum of 70% of the external field is excluded whereas at the front portion there is a maximum of 35% exclusion. Since the external magnetic field is greatly reduced by the diamagnetic shielding current for a large portion of the beam, the dominant drift mechanism for most of the beam is not $\vec{E} \times \vec{B}$ drifts. Only the edges of the beam drift through the field by the mechanism of $\vec{E} \times \vec{B}$ drifts. The rest of the beam propagates

through the field due to ion ballistic momentum.

For the simulation run with $\beta = 65$ (case 6 in Table 1) the ratio of the thermal velocity to the drift velocity is larger than the previous case (case 5). Thus the beam width increases more from thermal spreading (figure 12). Even though ϵ and β are smaller than case 5 the magnetic field is more effectively shielded out. The external magnetic field is totally excluded from a large portion of the back of the beam (figure 13). The rest of the interior of the beam maintains 75% exclusion. Two effects may be working together. A smaller collisionless skin depth, $\lambda_c = \frac{c}{\omega_{pe}}$, may force the shielding current to remain closer to the surface. The collisionless skin depth is half that of case 5. The other factor is the spreading of the plasmoid. The current profile is broader to the exterior of the beam than case 5 which allows complete magnetic shielding. Geometrical factors such as the ratio of the collisionless skin depth to the beam radius may be important in determining the amount of magnetic shielding in high β beams.

5 SUMMARY

In summary two dimensional electrostatic and electromagnetic PIC codes have been used to investigate plasma beam propagation across magnetic fields. The electrostatic simulations show that a plasma beam can propagate across magnetic fields via $E \times B$ drifts with $u_x \approx u_0$ if $\epsilon \gg (\frac{M}{m})^{\frac{1}{2}}$ and the ion gyroradius ρ_i of the beam is large. This is in agreement with theory (Peter and Rostoker 1982). There is little distortion of the beam. However loss of electrons and ions from charge layers at the edges of the beam appears and undulations in the potential are observed which reflect small oscillations in the beam drift velocity. Plasma beams with $\epsilon \approx (\frac{M}{m})^{\frac{1}{2}}$ propagate across magnetic fields with substantially reduced beam velocity u_x and extensive beam degradation. In early phases of injection the magnetic fields distort the beam causing reflection of ions and the formation of an asymmetric potential (Wessel and Robertson 1981). For beams with $\epsilon \ll (\frac{M}{m})^{1/2}$ the electrons and ions decouple at the magnetic field boundary and stop immediately.

The electrons turn around within a distance of ρ_e whereas the ions turn around within a distance on the order of $\frac{u_0}{\omega_{pi}}$ or ρ_i depending on how small ϵ is. On the other hand, the simulations of dense plasma beams with small ρ_i show that they are capable of penetrating several a_h into the magnetic field through to the Rayleigh-Taylor instability (Peter et. al. 1979). The high β beams penetrate in a markedly different mechanism. The electromagnetic simulations show that high β plasma beams shield out magnetic fields from the interior of the beam through the formation of diagmagnetic currents. It is this shielding which allows the beam to propagate across the magnetic field through ion ballistic momentum. The shielding depends on the ratio of λ_c to the beam width. As the beam with high β propagates, the magnetic fields eventually penetrate and then the polarization will be setup if $\epsilon \gg (\frac{M}{m})^{\frac{1}{2}}$. This should help the beam propagate by the $E \times B$ drift.

Acknowledgements

This work was based on the first author's thesis submitted to and accepted by the University of Texas at Austin in May 1985. We would like to thank Dr. H. Alfven, Dr. L. Lindberg, Dr. W. Peter, Dr. B. Newberger, and Dr. A. Fisher for their comments. Also acknowledged is the support given by the Internal Research Program of the Southwest Research Institute. This work was supported by Air Force Office of Scientific Research Contract F49620-86-K-0004 , National Science Foundation grant ATM 88-11128, the U. S. Department of Energy DE-FG05-80ET53088, and NASA NAGW-846.

References

Baker, D.A. & Hammel, J. E. 1962 *Phys. Rev. Letters* **8**, 157.

Birdsall, C. K. & Langdon, A. B. 1985 *Plasma Physics via Computer Simulation.* McGraw-Hill.

Bostick, W. H. 1956 *Phys. Rev.* **104**, 292.

Chapman, S. & Ferraro, V.C.A. 1931 *J. Geophys. Res.* **36**, 77.

Galvez, M. 1987 *Phys. Fluids* **30**, 2729.

Galvez, M. & Barnes C. 1988 *Phys. Fluids* **31**, 863.

Galvez, M., Gary, S. P., Barnes, C., & Winske, D. 1988 *Phys. Fluids* **31**, 1554.

Haerendel, G. & Sagdeev, R. Z. 1981 *Adv. Space Res.* **1**, 29.

Hockney, R. & Eastwood, J. W. 1981 *Computer Simulation Using Particles.* McGraw-Hill.

Humanic, D. G., Goede, H.,& Dawson, J. M. 1982 *Phys. Fluids* **25**, 271.

Ishizuka, H. & Robertson, S. 1982 *Phys. Fluids* **25**, 2353.

Lindberg, L. 1978 *Astrophys. and Space Sci.* **55**, 203.

Ott, E. and Manheimer, W. M. 1977 *Nucl. Fusion* **17**, 1057.

Papadopoulos, K., Mankofsky, A., & Drobot, A. 1988 *Phys. Rev. Lett.* **61**, 94.

Peter, W. 1981 Ph.D. dissertation, University of California, Irvine.

Peter, W., Ron, A., & Rostoker, N. 1979 *Phys. Fluids* **22**, 1471.

Peter, W. & Rostoker, N. 1982 *Phys. Fluids* **25**, 730.

Ripin, B. H., McLean, E. A., Manka, C. K., Pawley, C., Stamper, J. A., Peyser, T. A., Mostovych, A. N., Grun, J., Hassam, A. B., & Huba, J. D. 1987 *Phys. Rev. Lett.* **59**, 2299.

Schmidt, G. 1960 *Phys. Fluids* **3**, 961.

Sinelnikov, K. D. & Rutkevich, B. N. 1967 *Zh. Tekh. Fiz.* **37**, 56 [1967 *Sov. Phys.-Tech. Phys.* **12**,37].

Tajima, T. 1989 *Computational Plasma Physics.* Addison-Wesley.

Treumann, R. A. and Hausler, B. 1985 *Astrophys. Space Sci.* **110**, 371.

Wessel, F. & Robertson, S. 1981 *Phys. Fluids* **24**, 739.

Winglee, R. M. & Pritchett, P. L. 1987 *J. Geophys. Res.* **92**, 7689.

Winske, D. 1988 *J. Geophys. Res.* **93**, 2539.

Figure Captions

Figure 1 : Initial charge separation and resulting transverse electric field.

Figure 2 : Simulation geometry for two dimensional beam injection.

Figure 3 : Electron (3a,c) and ion (3b,d) particle plots for beam injection into a transverse magnetic field for the case of $\epsilon \gg (\frac{M}{m})^{\frac{1}{2}}$. Times are $4\omega_{pe}^{-1}$ and $7\omega_{pe}^{-1}$

Figure 4 : Electric potential plots for beam injection into a transverse magnetic field for the case of $\epsilon \gg (\frac{M}{m})^{\frac{1}{2}}$ where 4a and 4b are times $4\omega_{pe}^{-1}$ and $7\omega_{pe}^{-1}$ respectively.

Figure 5 : Electron (5a,c,e,g) and ion (5b,d,f,h) particle plots for beam injection into a transverse magnetic field for the case of $\epsilon \approx (\frac{M}{m})^{\frac{1}{2}}$. Times are 5.0, 7.5, 8.75, and $12.5\omega_{pe}^{-1}$ down the figure.

Figure 6 : Electric potential plots for beam injection into a transverse magnetic field for the case of $\epsilon \approx (\frac{M}{m})^{\frac{1}{2}}$ with times 5, 8.75, and $12.5\omega_{pe}^{-1}$ down the figure.

Figure 7 : Electron (7a,c,e,g) and ion (7b,d,f,h) particle plots for the wide beam injection into a transverse magnetic field. Times are 20, 30, 40, and $50\omega_{pe}^{-1}$

Figure 8 : E_y field plots for the wide beam injection into a transverse magnetic field. Times are 20, 30, 40, and $50\omega_{pe}^{-1}$

Figure 9 : Electron (9a) and ion (9b) particle plots at time $60\omega_{pe}^{-1}$ in the case of $\beta = 130$ for the electrons and ions when the entire beam is embedded in the magnetic field.

Figure 10 : Diamagnetic current, J_x, profile across the beam for $\beta = 130$ at time $60\omega_{pe}^{-1}$

Figure 11 : Magnetic field contours for $\beta = 130$, indicating beam diamagnetism and field penetration for time $60\omega_{pe}^{-1}$. Notice nonuniformity of field penetration.

Figure 12 : Electron (12a) and ion (12b) particle plots for time $100\omega_{pe}^{-1}$ in the case of $\beta = 65$ for the electrons and ions when the entire beam is embedded in the magnetic field.

Figure 13 : Magnetic field contours for $\beta = 65$, indicating beam diamagnetism and field penetration at time $100\omega_{pe}^{-1}$. Total exclusion of external field at back of beam.

Case	ϵ	β	$u_0/\Delta\omega_{pi}$	ρ_i/Δ	λ_D/Δ	M/m
1	328.7	0.8	3.9	70	0.3	10
2	3.15	0.94	3.9	5.68	0.3	10
3	2.0	0.49	140	140	0.3	400
4	92.02	0.09	1.05	10.0	0.3	10
5	3278	128.5	1.21	69.3	0.3	25
6	1639	62.9	0.60	24.5	0.3	25

Table 1

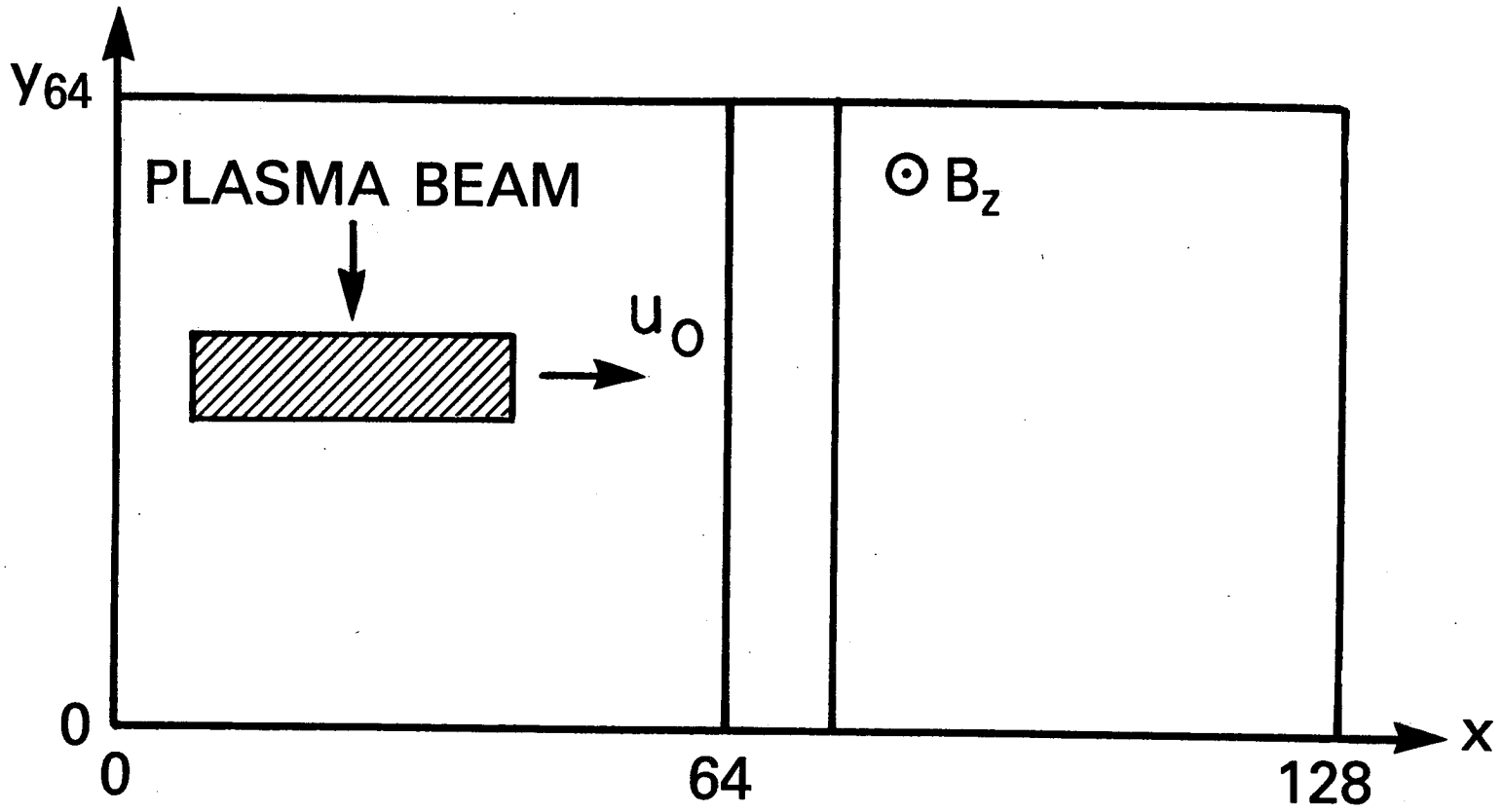

Fig. 1

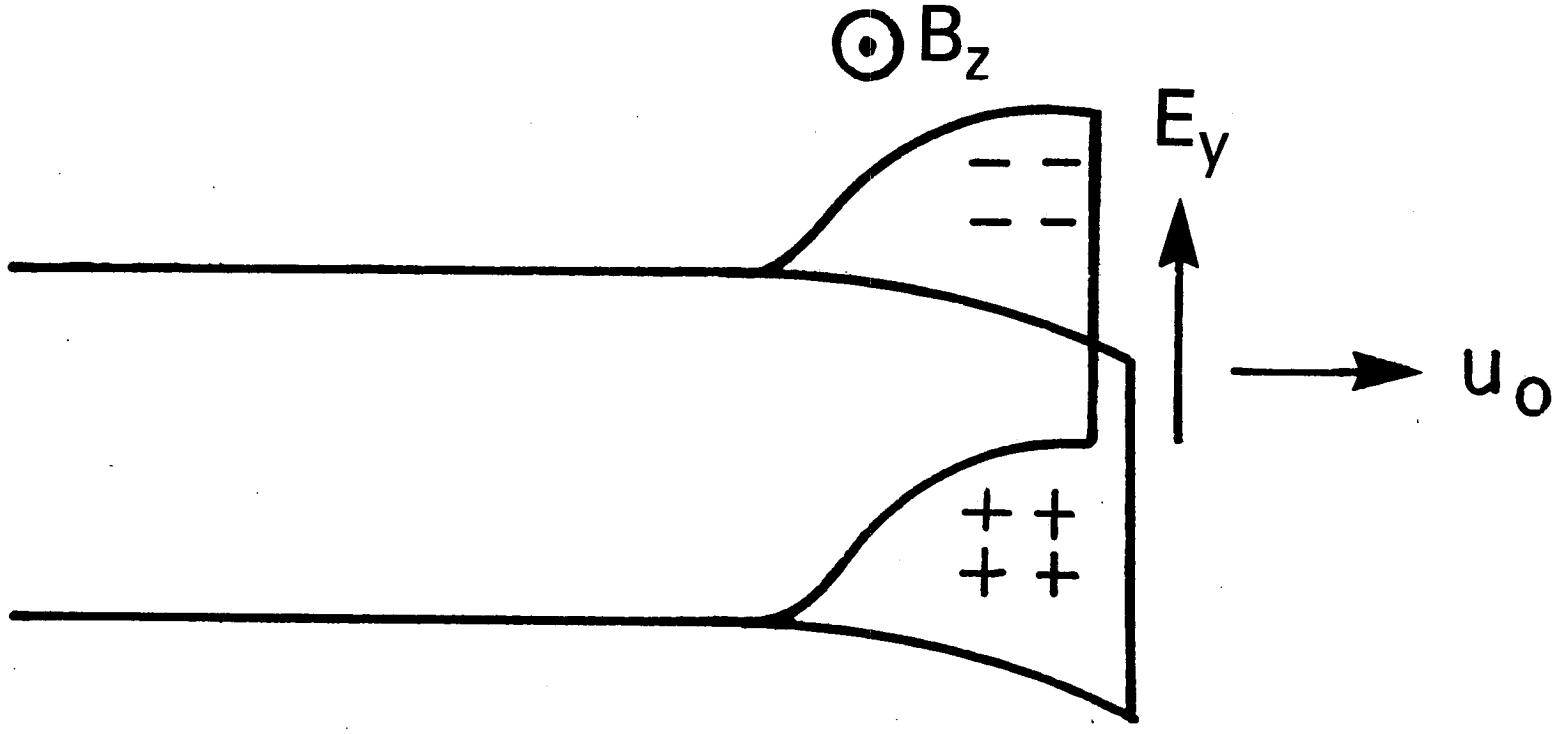

Fig. 2

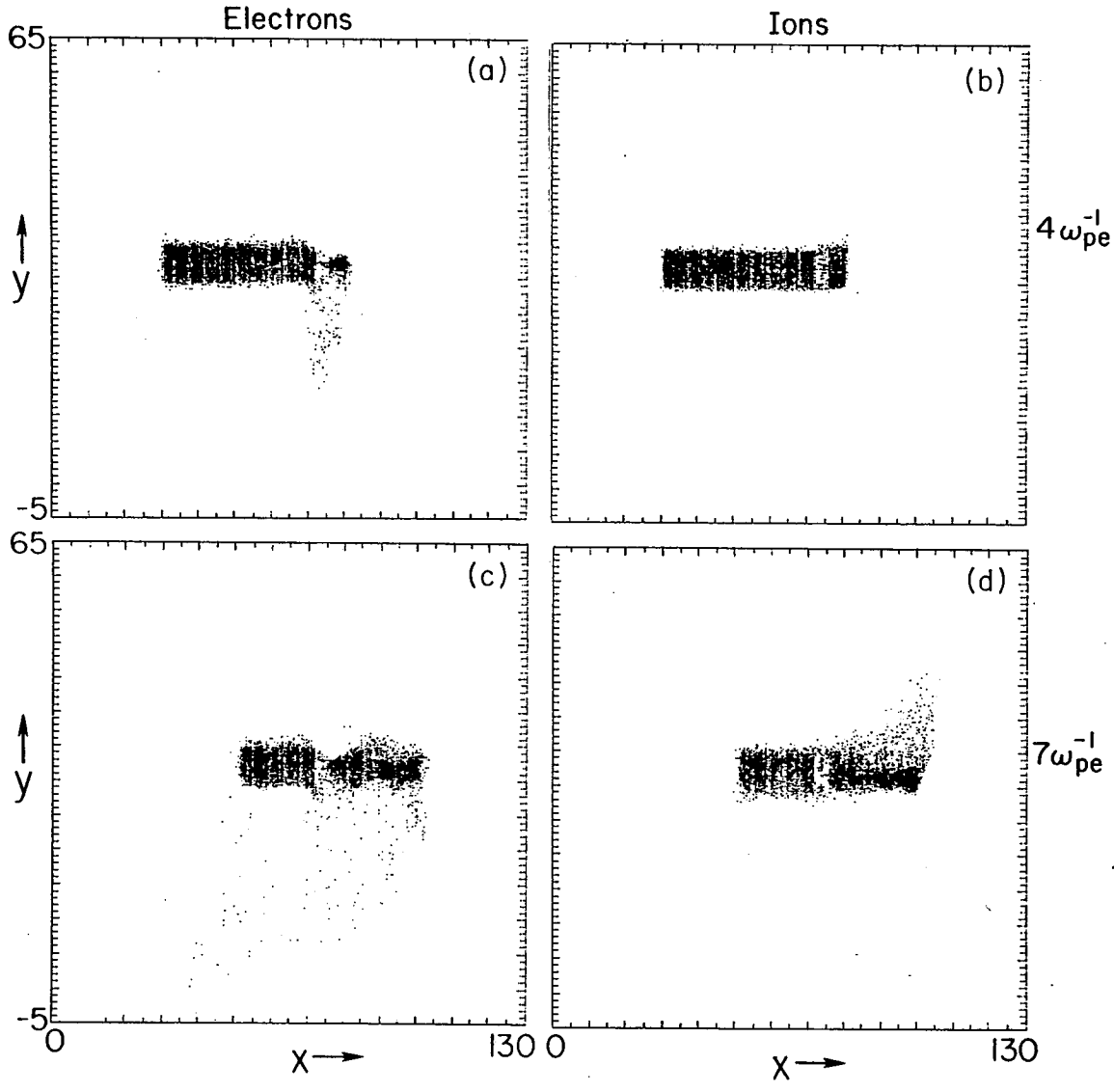
Electrons
Ions
65
(a)
(b)
y
-5
$4\omega_{pe}^{-1}$
65
(c)
(d)
y
$7\omega_{pe}^{-1}$
-5
0
130
X
0
130
X

Fig. 3

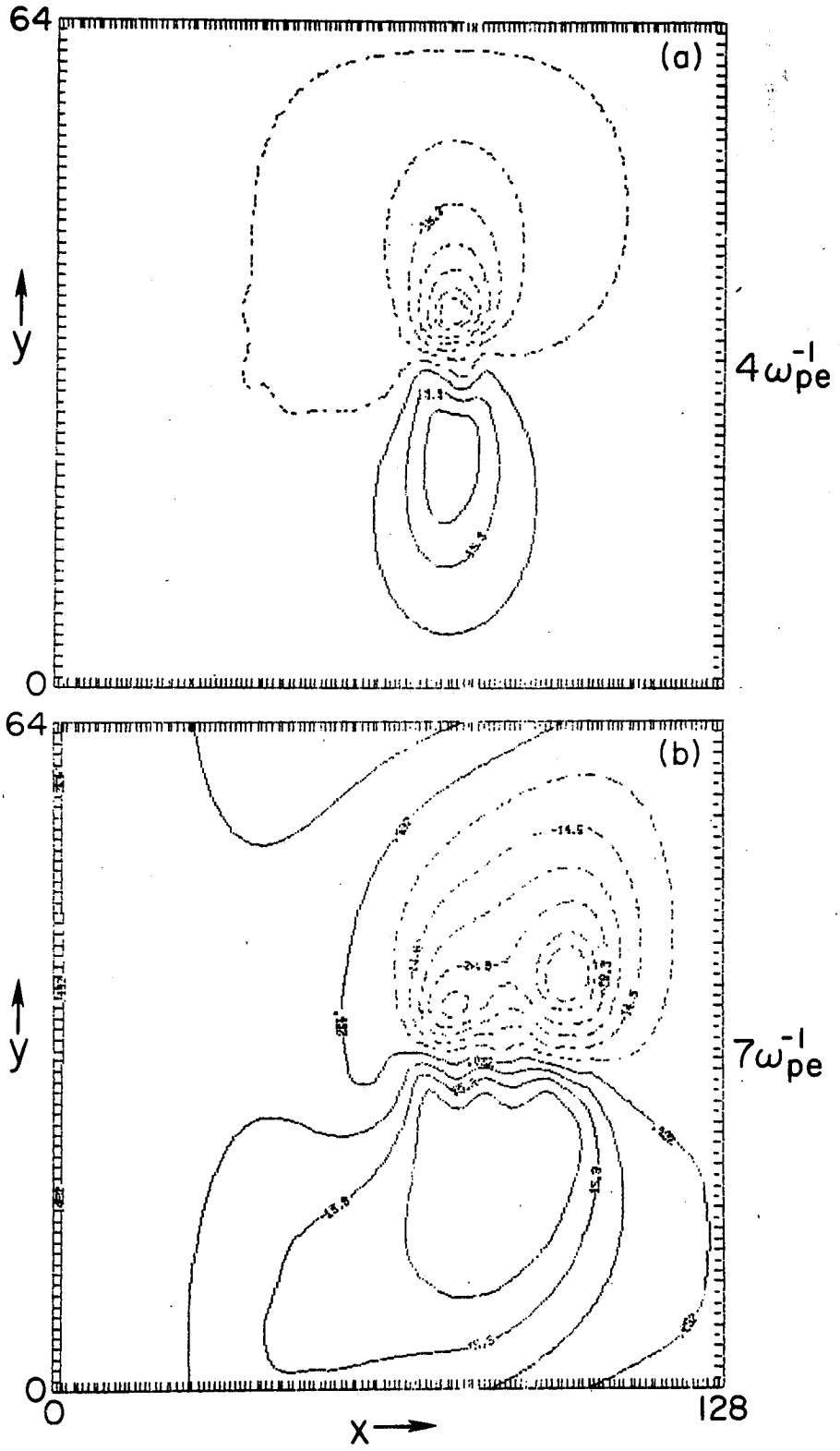

Fig. 4.

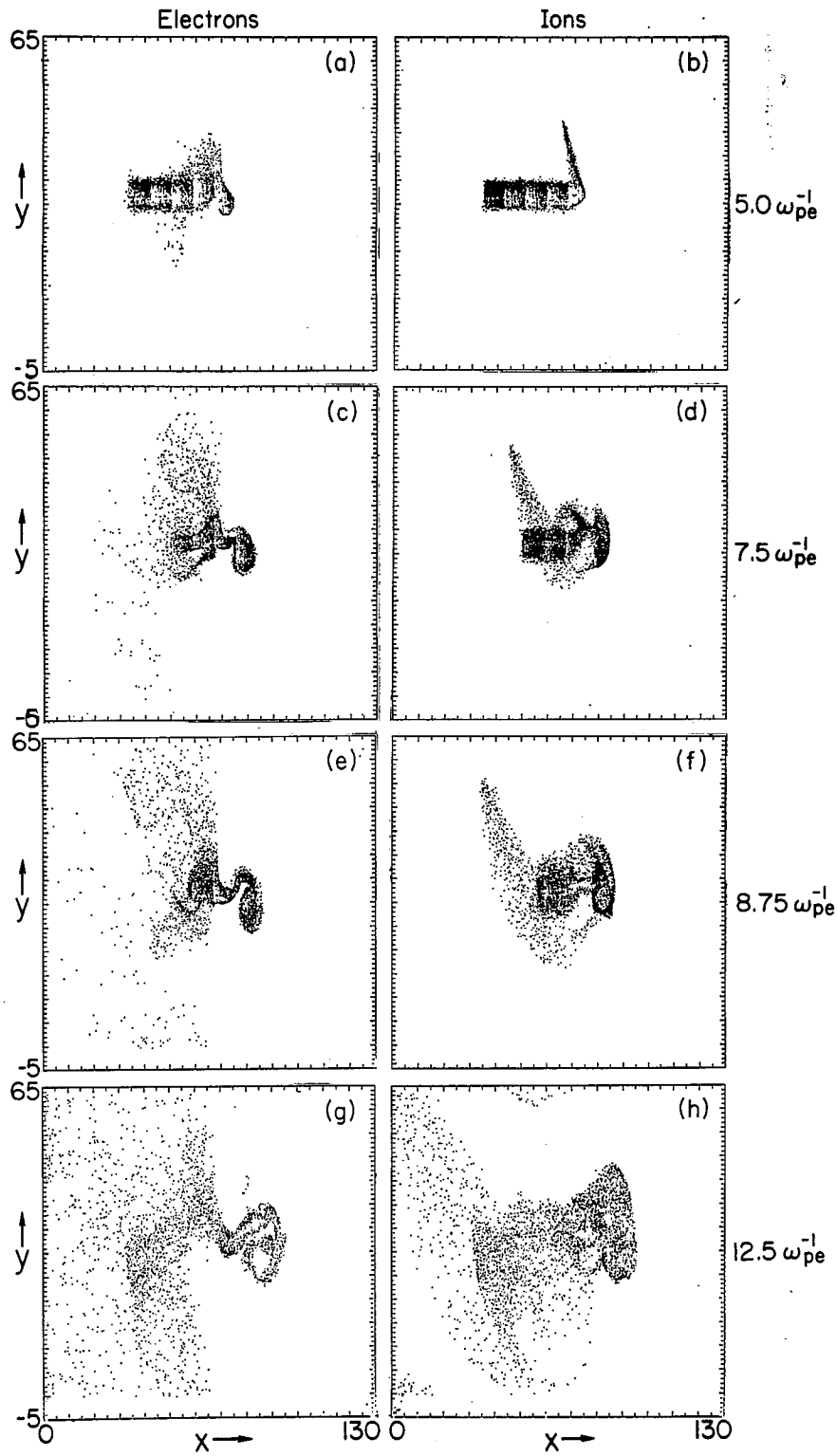
Electrons
Ions
(a)
(b)
(c)
(d)
(e)
(f)
(g)
(h)
65
-5
-6
y
x
0
130
5.0 ω_{pe}^{-1}
7.5 ω_{pe}^{-1}
8.75 ω_{pe}^{-1}
12.5 ω_{pe}^{-1}

Fig. 5

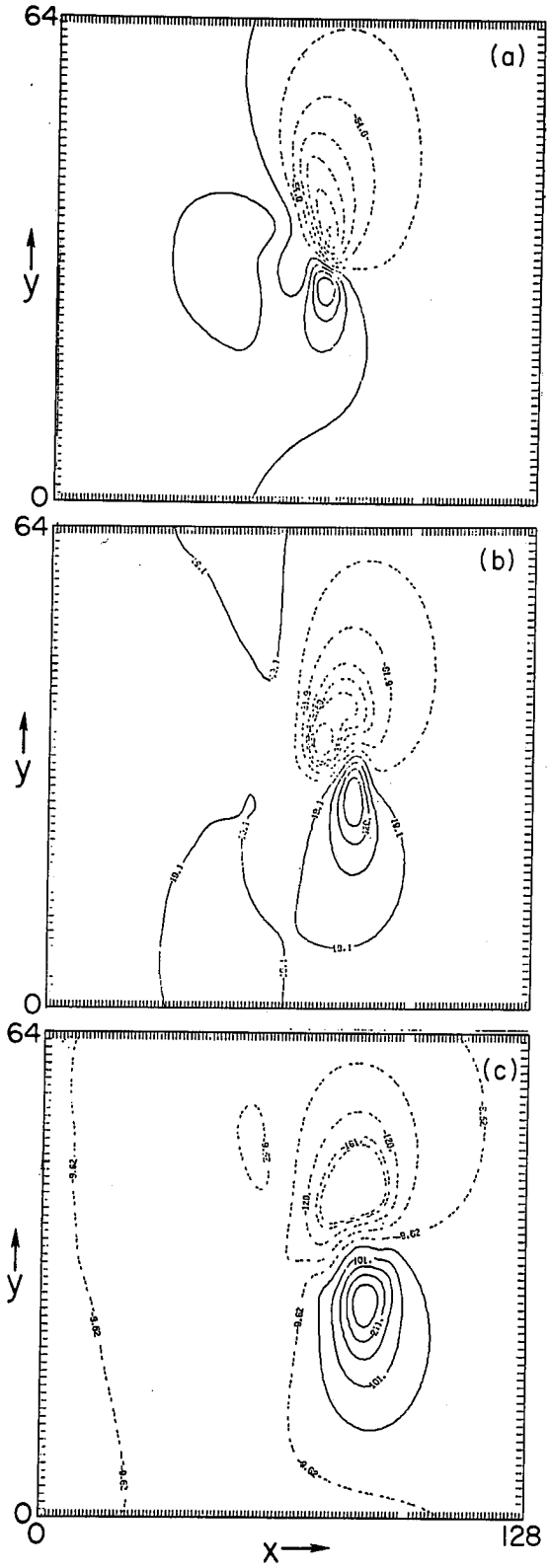

Fig. 6

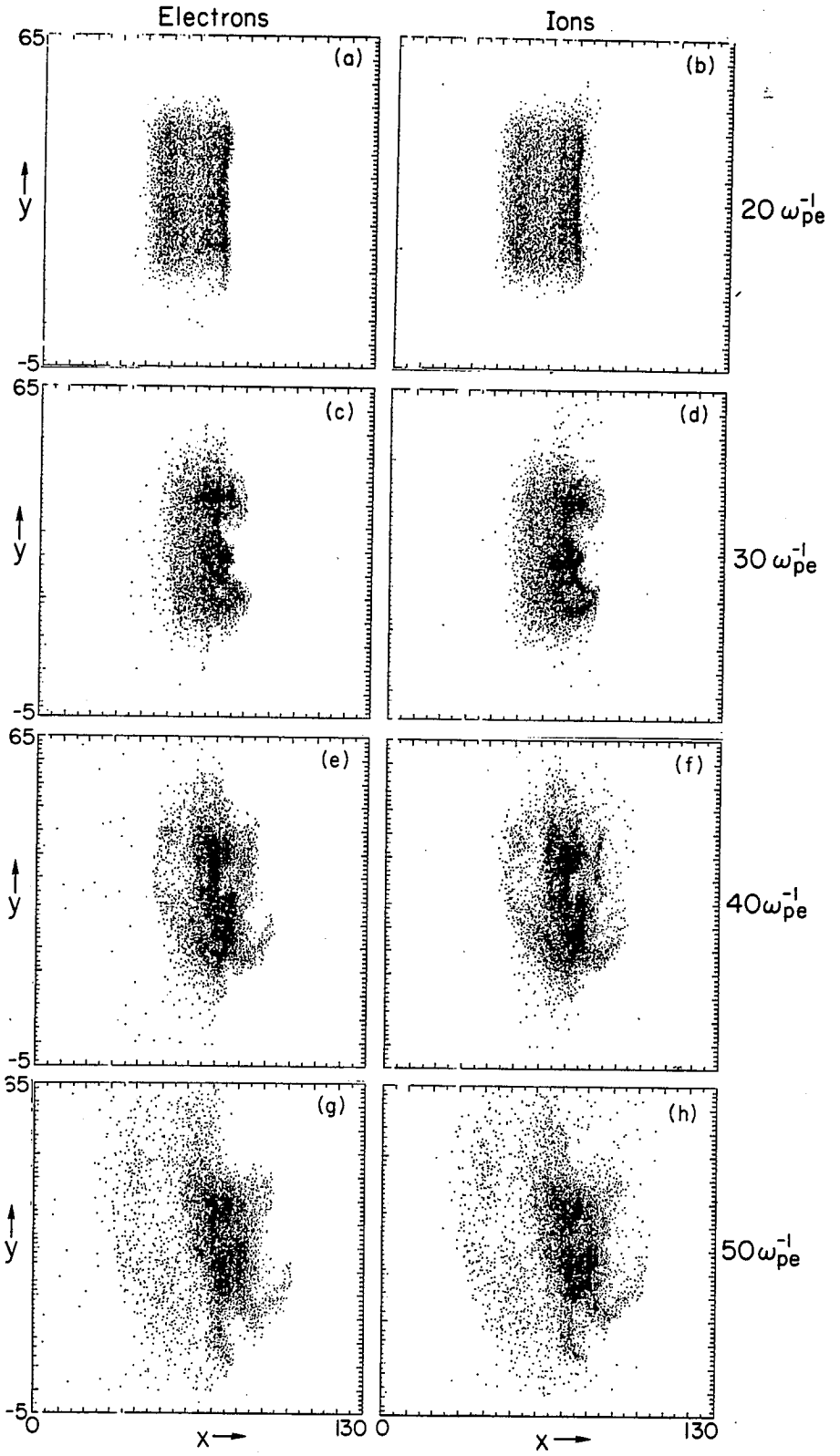
Electrons
Ions
65
-5
(a)
(b)
(c)
(d)
(e)
(f)
(g)
(h)
y
x
0
130
20 ω⁻¹pe
30 ω⁻¹pe
40ω⁻¹pe
50ω⁻¹pe

Fig. 7

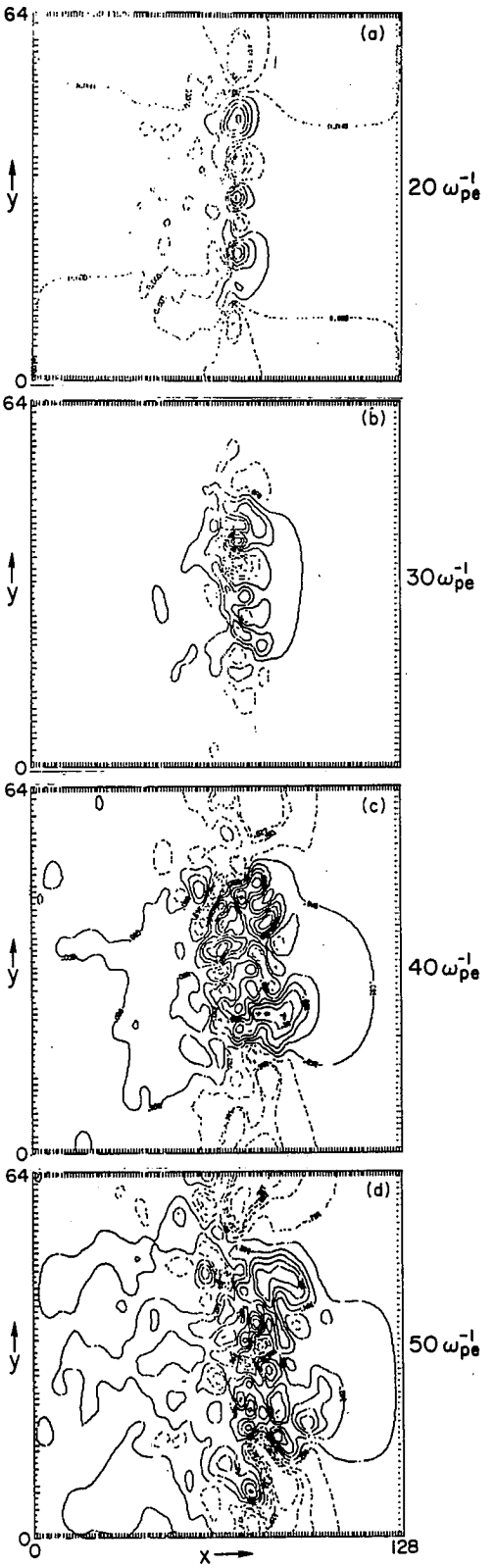
64
(a)
y
0
20 ω_pe^-1
64
(b)
y
0
30 ω_pe^-1
64
0
(c)
y
0
40 ω_pe^-1
64
(d)
y
0
50 ω_pe^-1
0
x
128

Fig. 8

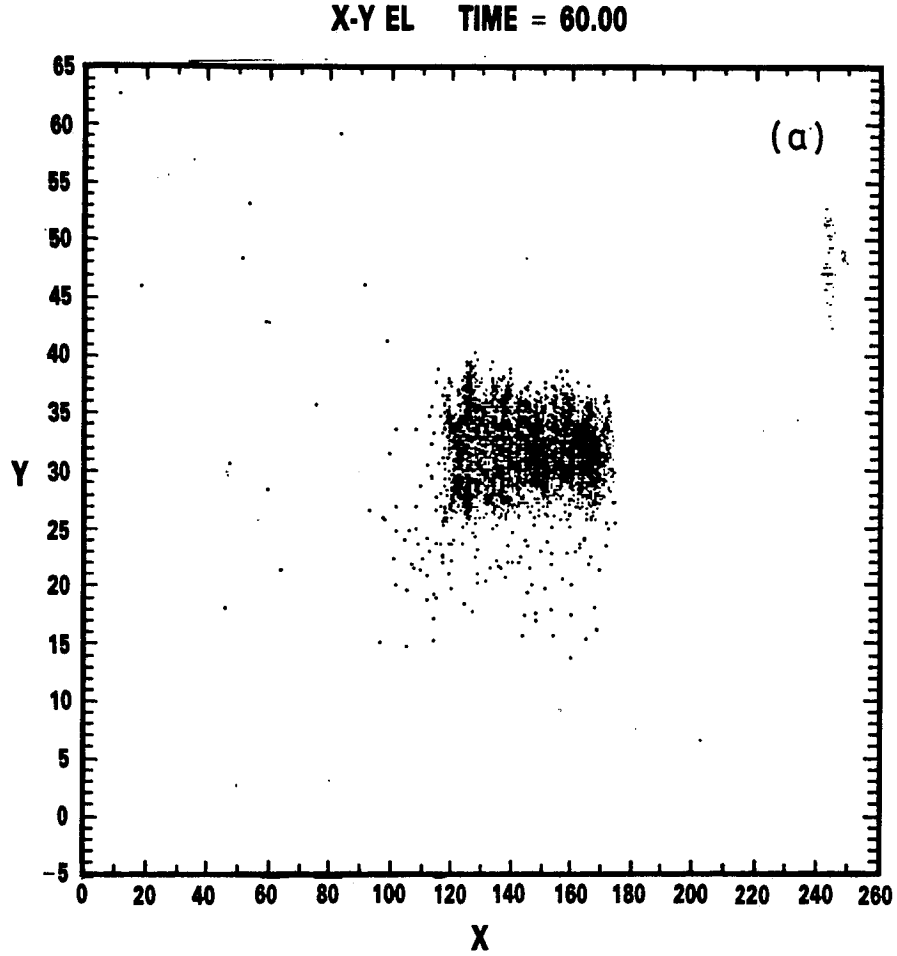
X-Y EL TIME = 60.00
(a)
Y
X
65
60
55
50
45
40
35
30
25
20
15
10
5
0
-5
0
20
40
60
80
100
120
140
160
180
200
220
240
260

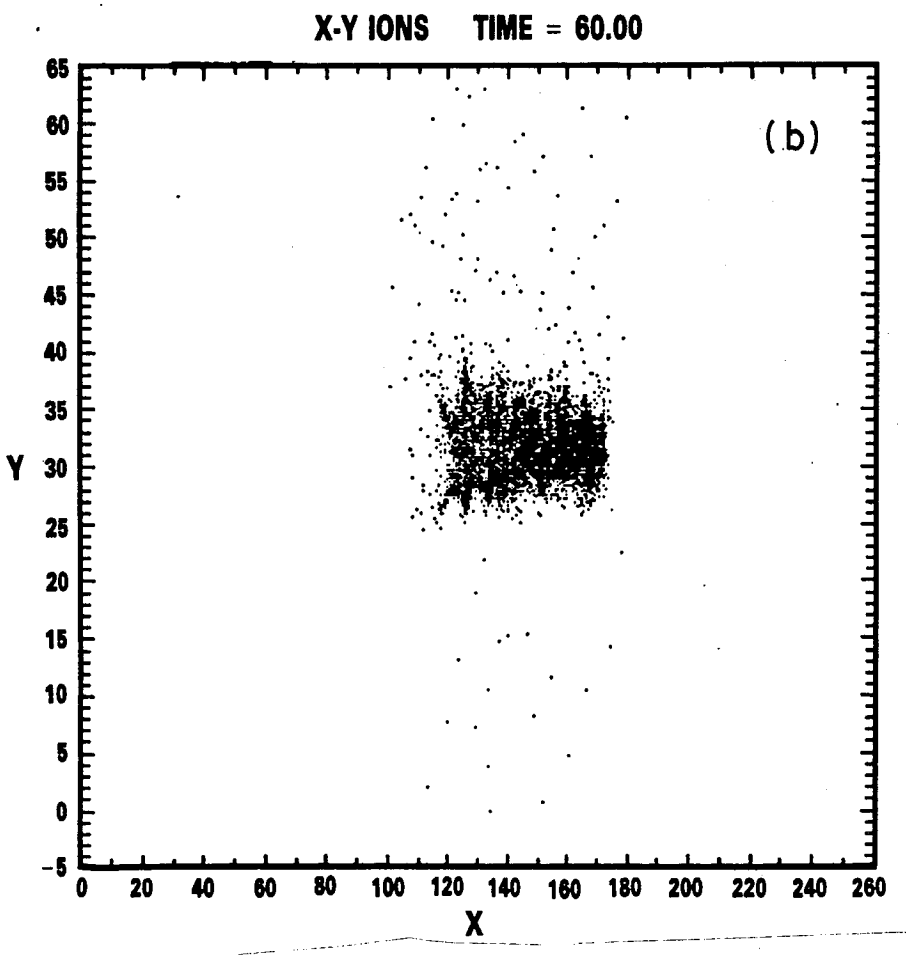
X-Y IONS TIME = 60.00
(b)
Y
X
65
60
55
50
45
40
35
30
25
20
15
10
5
0
-5
0
20
40
60
80
100
120
140
160
180
200
220
240
260

Fig. 9

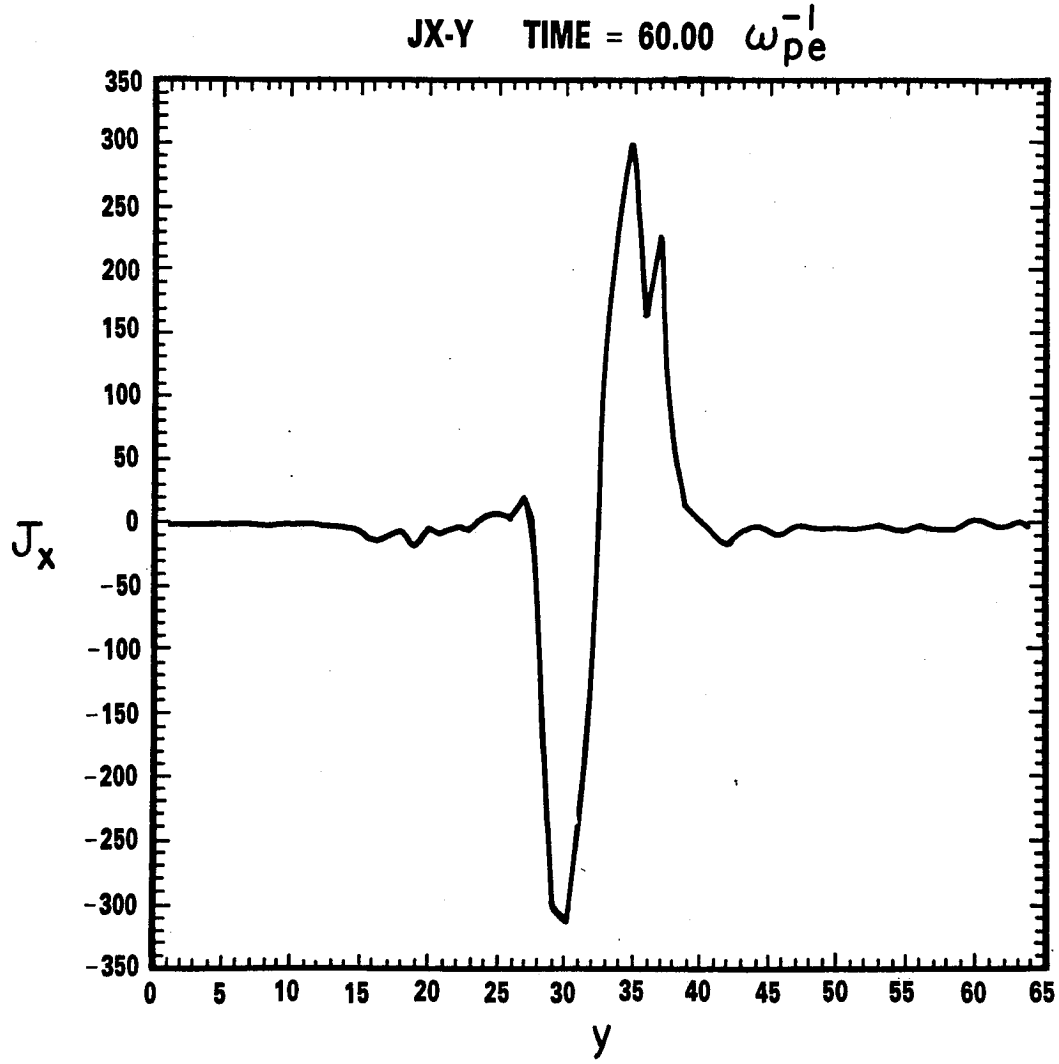
JX-Y TIME = 60.00 ω_{pe}^{-1}
J_x
y
350
300
250
200
150
100
50
0
-50
-100
-150
-200
-250
-300
-350
0
5
10
15
20
25
30
35
40
45
50
55
60
65

Fig. 10

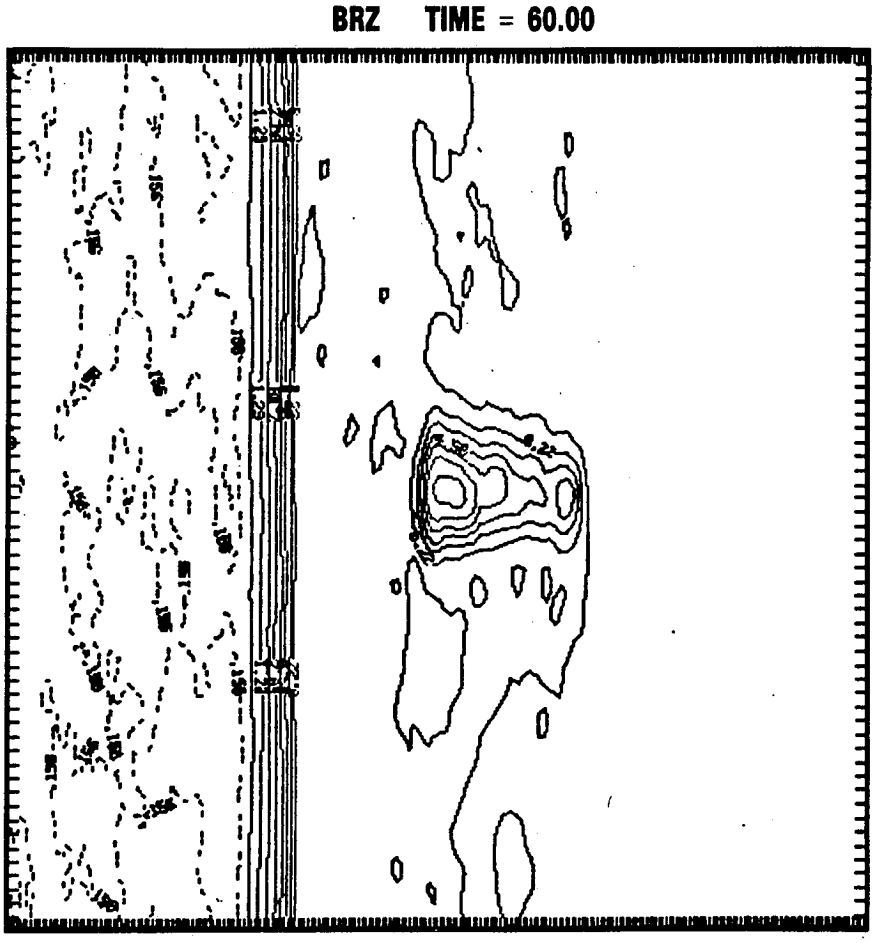

Fig. 11

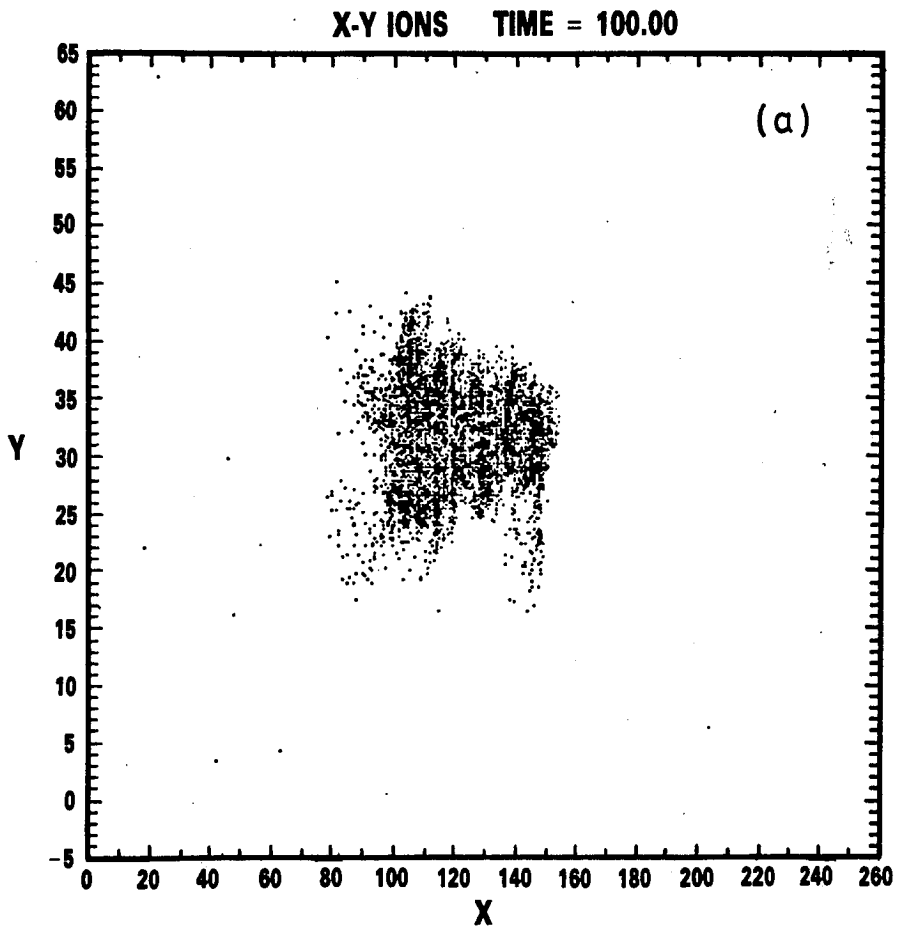
X-Y IONS TIME = 100.00
(a)
Y
X
65
60
55
50
45
40
35
30
25
20
15
10
5
0
-5
0
20
40
60
80
100
120
140
160
180
200
220
240
260

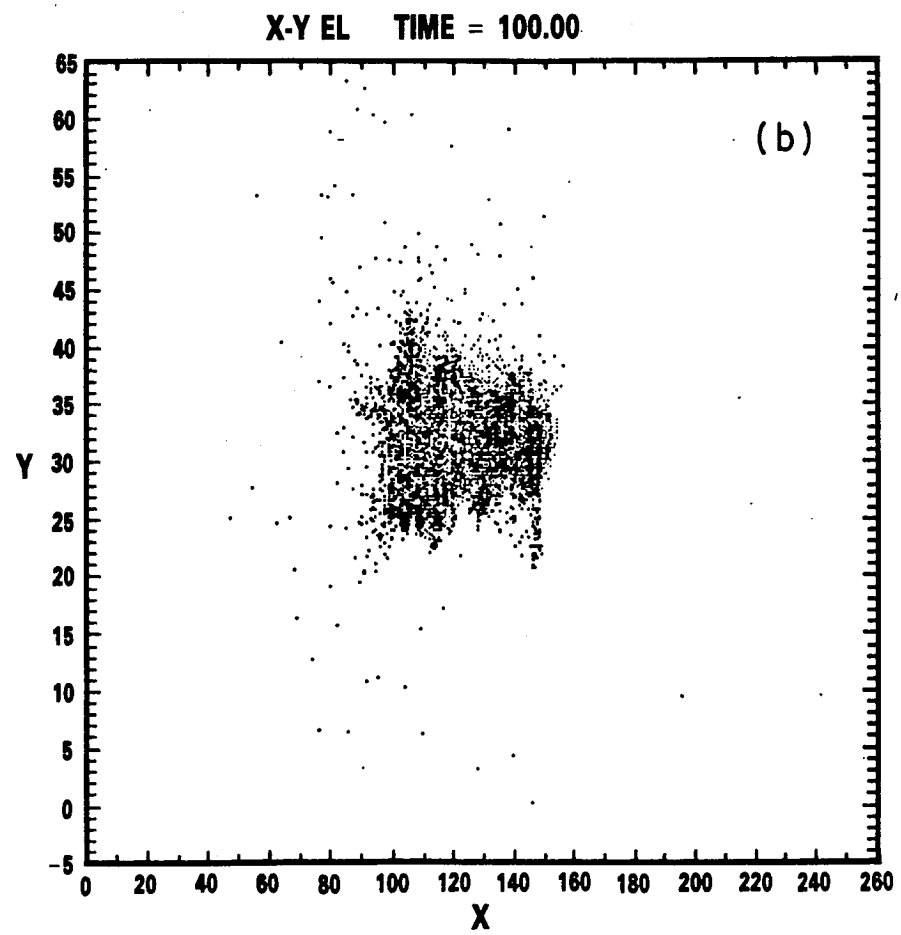
X-Y EL TIME = 100.00
(b)
Y
X
65
60
55
50
45
40
35
30
25
20
15
10
5
0
-5
0
20
40
60
80
100
120
140
160
180
200
220
240
260

Fig. 12

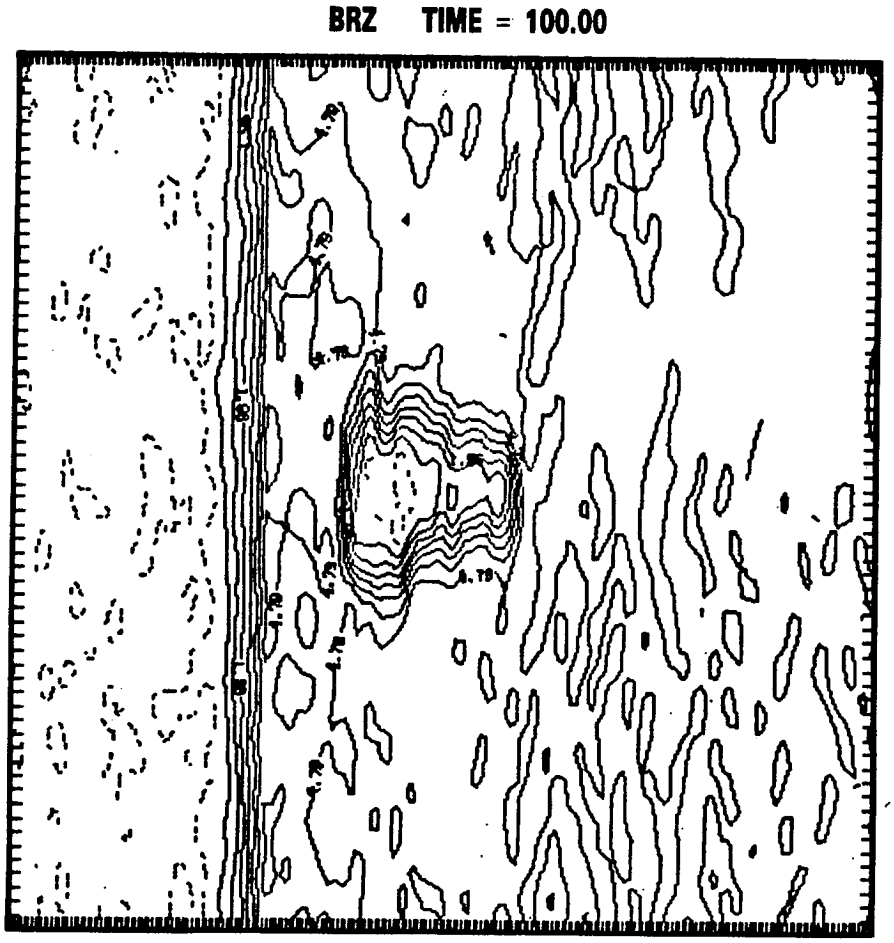

Fig. 13